Chinese Chemical Letters 35 (2024) 109254

Contents lists available at ScienceDirect

Chinese Chemical Letters

journal homepage: www.elsevier.com/locate/cclet

Feedback enhanced tumor targeting delivery of albumin-based nanomedicine to amplify photodynamic therapy by regulating AMPK signaling and inhibiting GSTs

Jiaqi Huang[a], Renjiang Kong[a], Yanmei Li[a], Ni Yan[a], Yeyang Wu[a], Ziwen Qiu[a], Zhenming Lu[a], Xiaona Rao[b], Shiying Li[b,*], Hong Cheng[a,*]

[a] School of Biomedical Engineering & Guangdong Provincial Key Laboratory of Construction and Detection in Tissue Engineering, Southern Medical University, Guangzhou 510515, China
[b] School of Pharmaceutical Sciences, Guangzhou Medical University, Guangzhou 511436, China

ARTICLE INFO

Article history:
Received 8 September 2023
Revised 26 October 2023
Accepted 27 October 2023
Available online 28 October 2023

Keywords:
Human serum albumin
Drug delivery
Reactive oxygen species
Positive feedback uptake
Oxidative damage

ABSTRACT

Oxidative therapies receive a limited antitumor efficiency due to the insufficient reactive oxygen species (ROS) levels at focal sites and the evolvement of antioxidant defense systems. Herein, we develop an albumin-based nanomedicine to co-deliver chlorin e6 (Ce6) and COH-SR4 (CS), which can simultaneously enhance the yield and lethality of intracellular ROS for amplified photodynamic therapy (PDT). In which, CS acts as both an activator of AMP-activated protein kinase (AMPK) and an inhibitor of glutathione *S*-transferases (GSTs). Benefiting from it, the prepared HSA-Ce6@COH-SR4 (HCCS) enables positive feedback uptake by promoting AMPK phosphorylation, leading to rapid and extensive tumor accumulation of drugs. As a result, HCCS obviously increases the ROS production to elevate intracellular oxidative stress. Furthermore, HCCS can inhibit GSTs to disturb the antioxidant defense system of tumor cells, intensifying the oxidative damage of ROS. Ultimately, the PDT of HCCS is significantly strengthened by improving the ROS yield and lethality, which greatly declines the proliferation of breast cancer *in vivo*. This study may open a window in the development of drug co-delivery system for enhanced oxidative therapy of tumors.

In the past decades, photodynamic therapy (PDT) has gained increasing attention as a promising approach in tumor treatment [1,2]. Photosensitizers can convert oxygen into highly oxidizing reactive oxygen species (ROS) to kill tumor cells after being excited by a specific light. PDT offers the advantage of tumor targeting by selecting the location of light, minimizing damages to normal tissues. Moreover, the transient nature of ROS allows for the avoidance of long-term side effects, as ROS is rapidly deactivated after exerting its cytotoxic effects. However, most photosensitizers are hydrophobic with poor pharmacokinetic profiles, causing a limited bioavailability and low ROS yield. In order to improve it, many strategies have been proposed to increase the ROS production, such as utilizing targeted carriers to deliver photosensitizers, increasing oxygen supply [3], reducing oxygen consumption [4–6], and prolonging the irradiation time [7]. But uneven oxygen partial pressures and overlong light irradiation *in vivo* might cause an excessive production of ROS locally, inducing an unpredictable oxidative damage on normal tissues around tumors. Additionally, metabolic abnormalities of tumor cells results in impaired redox regulation and the accumulation of excessive oxidative stress in tumor microenvironments, leading to the development of resistance to oxidative therapies. Thus, for maximizing PDT efficacy, it is more clinically significant to increase the ROS generation by promoting the targeted delivery of photosensitizers and simultaneously enhance the lethality of ROS to tumor cells by disturbing the endogenous antioxidant defense systems [8].

Human serum albumin (HSA) is an endogenous plasma protein in the human body, which plays a key role in transporting various substances [9–11]. Also, it is known as an ideal drug carrier because it has an excellent biocompatibility and drug-carrying properties, which can combine with different drugs through covalent binding and hydrophobic interaction [12–14]. Besides, HSA served as a nutrient can be actively internalized by cells through macropinocytosis pathway. The recognition of HSA and secreted protein acidic and rich in cysteine (SPARC) on tumor cells might accelerate the intracellular drug delivery [15,16]. Of note, AMP-activated protein kinase (AMPK) is a key enzyme involved in cellular energy metabolism, serving as a cell energy sensor.

* Corresponding authors.
E-mail addresses: lisy-sci@gzhmu.edu.cn (S. Li), chengh@smu.edu.cn (H. Cheng).

https://doi.org/10.1016/j.cclet.2023.109254
1001-8417/

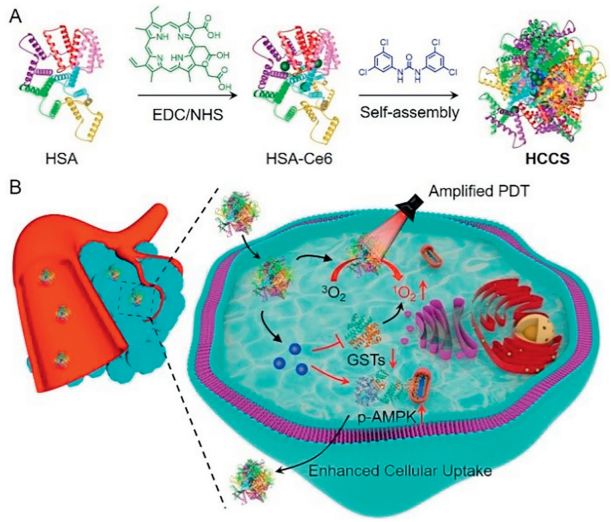

Scheme 1. Preparation and proposed mechanism of HCCS for enhanced PDT. (A) The preparation process of HSA-Ce6@COH-SR4 (HCCS) based on HSA, Ce6 and COH-SR4. (B) Intravenously injected HCCS was enriched in tumor tissues and internalized by tumor cells. The released COH-SR4 could activate the phosphorylation of AMPK (p-AMPK) to promote the positive feedback uptake of HCCS. COH-SR4 could inhibit the activity of GSTs to interrupt the anti-oxidation defense system, enhancing the oxidative damage and amplifying the PDT of tumor cells.

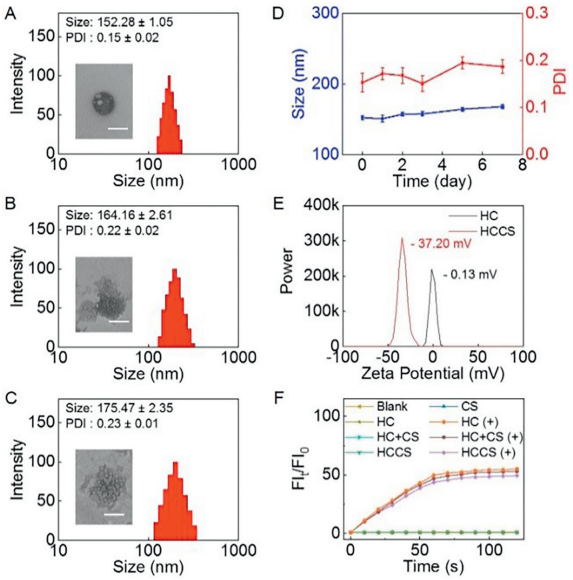

Fig. 1. Preparation and characterization of HCCS. Particle size distribution and TEM image of nanomedicine with the feed ratio of CS to Ce6 at (A) 1:1, (B) 1.5:1 and (C) 2:1. Scale bar: 100 nm. (D) Particle size and PDI variations of HCCS over 7 days. (E) Zeta potential of HC and HCCS. (F) ROS generation capabilities of HC, CS, HC + CS, and HCCS with or without light illumination ($n = 3$). Mean ± standard deviation (SD).

Interestingly, researches have shown that the activation of AMPK signaling pathway can effectively enhance the uptake of albumin-based nanomedicine [17–19]. Therefore, it is a prospective tactic to increase photosensitizer delivery efficiency by construction of an albumin-based carrier to load AMPK activators, realizing the positive feedback uptake of photosensitizers.

COH-SR4 (CS), as a kind of AMPK activators with strong hydrophobicity [20], can induce HSA to assemble into nanoparticles through hydrophobic interaction [21,22]. Meanwhile, CS is reported for tumor therapy by inhibiting glutathione *S*-transferases (GSTs) [23]. The upregulation of GSTs is a common feature of many tumors, which participate in many tumorigenic processes including cell proliferation and drug resistance. More importantly, GSTs as an important antioxidant enzyme regulate the stress induced signal pathway, which can catalyze the conjugation of glutathione (GSH) to electrophilic compounds [24–27]. Therefore, CS can not only act as AMPK activator to promote cell uptake of photosensitizers, but also used as GSTs inhibitor to destroy the antioxidant defense systems of tumors, showing a compelling advantage to synergize with PDT.

In view of the above, we herein developed a drug co-delivery system based on HSA to transport photosensitizer and CS for enhanced photodynamic tumor therapy. First, the photosensitizer of chlorin e6 (Ce6) was linked to HSA by covalent binding to prepare HSA-Ce6 (HC) (Scheme 1A). Then the hydrophobic CS could be encapsulated into HC to assemble into stable nanoparticles (HSA-Ce6@COH-SR4, abbreviated as HCCS). HCCS exhibited targeted enrichment in tumor tissue, followed by initial uptake by tumor cells. The presence of COH-SR4 offered dual functionality (Scheme 1B). On the one hand, it activated AMPK phosphorylation to further promote the uptake of HCCS by tumor cells, establishing a positive feedback loop. On the other hand, CS inhibited GSTs activity and disrupted the antioxidant defense system of tumor cells, which would reduce the consumption of ROS and enhance the lethality of PDT to tumors. Consequently, HCCS demonstrated an enhanced PDT effect to effectively inhibit tumor growth. This nanomedicine, fabricated through hydrophobic drug-induced assembly with albumin, exhibited excellent biocompatibility and significant therapeutic benefit, providing a novel approach for efficient and safe tumor treatment.

Prior to preparing HCCS, Ce6 was covalently bound to HSA to obtain HC. Then we took advantage of the hydrophobic nature of CS to fabricate nanoparticles with varying particle sizes and morphologies by adjusting feed ratios of CS to Ce6. The particle size distributions were analyzed using dynamic light scattering (DLS), as depicted in Figs. 1A–C, while the morphologies of particles formed under different ratios were observed *via* transmission electron microscopy (TEM). Among which, the assembly prepared at 1:1 was found to have more regular shape, narrow size distribution and lower PDI value (Fig. 1A). Moreover, the average size and PDI had no significant changes in aqueous solution for one week (Fig. 1D), indicating a fairly good stability. Although HC could also form into nanoparticles, it was found to have a loose structure and increased size distribution (Fig. S1 in Supporting information). Subsequently, the potentials of HC and HCCS were measured (Fig. 1E). The obvious difference of zeta potential demonstrated the successful loading of CS on HC. In addition, the zeta potential of nanomedicine became much more negative after assembly, which would reduce the protein adsorption in blood circulation. By using high performance liquid chromatography (HPLC) and ultraviolet–visible spectroscopy (UV–vis), the drug loading rates of CS and Ce6 in HCCS were measured to be 1.2% and 2.3% respectively (Fig. S2 in Supporting information). Taken together, CS and HC were able to assemble into negatively charged nanoparticles with favorable stability, which were named as HCCS for follow-up study. Furthermore, the efficiency of ROS generation by HCCS was assessed using the singlet oxygen sensor green (SOSG) probe (Fig. 1F). Notably, under light illumination, no significant difference was observed in the ROS generation efficiency between HCCS and HC, suggesting that the assembly process had no appreciable impact on the ROS generation capability. Besides, with the prolonged time of light exposure, the fluorescence intensity of SOSG was sharply increased immediately, illustrating a rapid ROS production by HCCS.

One of the design intentions of HCCS was to improve the delivery efficiency photosensitizers. To confirm it, the cellular uptake

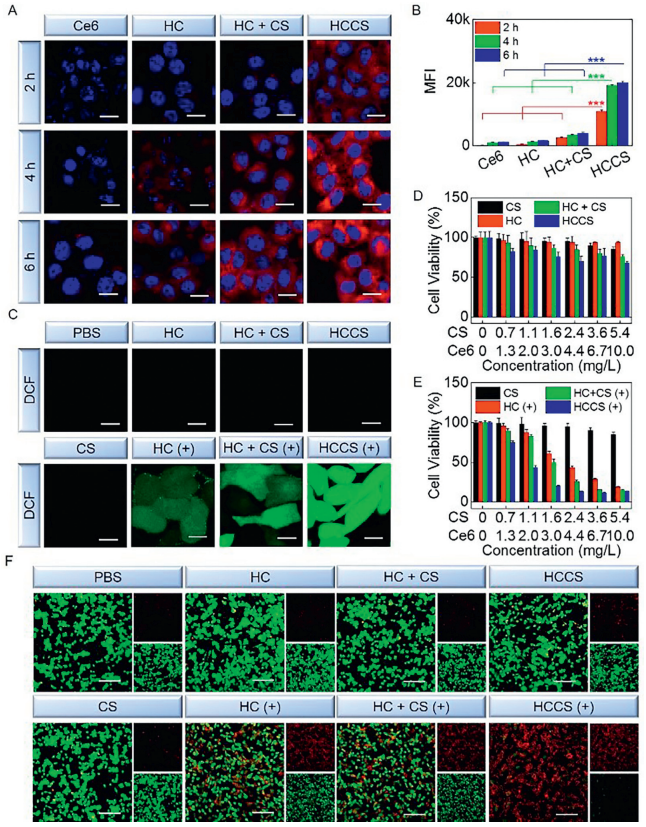

Fig. 2. Cellular uptake and anti-tumor effect *in vitro*. (A) CLSM images and (B) quantitative flow cytometry analysis of cellular uptake behaviors of 4T1 cells following treatment with Ce6, HC, HC + CS and HCCS for 2, 4 or 6 h ($n = 3$). Scale bar: 10 μm. (C) CLSM images showing intracellular ROS production in 4T1 cells following drug incubation. Scale bar: 10 μm. MTT assay of 4T1 cells incubated with gradient concentrations of CS, HC, HC + CS and HCCS (D) in the darkness and (E) in the presence of light. (F) Live/dead cell staining of 4T1 cells incubated with HC, CS, HC + CS and HCCS in the presence or absence of light. Scale bar: 100 μm. Mean ± SD. $^{***}P < 0.001$ was tested *via* a Student's *t*-test.

behavior of 4T1 cells was assessed after incubation with different drugs (Fig. 2A). Among the first three groups, 4T1 cells treated with HC + CS exhibited the strongest red fluorescence, while the cells treated with Ce6 showed the weakest red fluorescence. These findings suggested that HC had a higher internalization rate compared to free Ce6, and the internalization was further enhanced after CS incubation. There were two possible reasons for this results. First, HSA mimicked a nutrient, allowing it to enter the cell through macropinocytosis. Second, the modification of HSA might enhance the water solubility of the photosensitizer, making it more easily to be taken up by tumor cells. Moreover, CS further increased the cellular uptake of HC, which might result from AMPK activation. Excitingly, 4T1 cells treated with HCCS displayed significantly stronger red fluorescence than those treated with HC + CS, indicating a highly improved drug delivery efficiency in cell level. This phenomenon could be attributed to CS encapsulation within the albumin nanomedicine. Upon AMPK activation, the uptake of albumin nanomedicine increased, further facilitating the internalization of CS and AMPK activation in a positive feedback loop of cell uptake behavior. Flow cytometry was used for further verification of this uptake (Fig. 2B). The results demonstrated that, under the same incubation time, CS really promoted the uptake of HC by 4T1 cells, and HCCS dramatically increased the cell uptake compared to other groups. More precisely, after incubation for 6 h under the same condition, the fluorescence intensity of 4T1 cells treated by HC + CS was nearly 2 times higher than that of treated by HC only. Furthermore, the intracellular fluorescence of HCCS group was about 4-fold and 10-fold stronger than that of in HC + CS and HC groups respectively. Collectively, these experimental findings provided powerful evidence for the rapid internalization of HCCS by cells through a positive feedback mechanism.

The ultimate goal of HCCS was to maximize the cellular oxidative stress for enhanced PDT. In order to detect the intracellular ROS levels, 4T1 cells after various treatments were cultured with DCFH-DA and the cellular fluorescence was imaged by confocal laser scanning microscopy (CLSM) (Fig. 2C). Although HC and HCCS were tested to have a comparable photodynamic property in aqueous solution, the former generated very limited ROS in cells. In contrast, 4T1 cells treated with HCCS displayed blindingly bright green fluorescence under identical light conditions, indicating a great efficiency in ROS production. Besides, the addition of CS was verified to facilitate the ROS production by HC. Thus, it was guessed that there must be two potential factors contribute to this difference. First, the cellular uptake of HCCS multiplied benefiting from CS, which caused a much more concentration of photosensitizers in 4T1 cells. Second, the inhibition of GSTs activity by CS might reduce the loss of ROS generated by HC, resulting in an increased oxidative stress in 4T1 cells.

The efficient drug delivery and photodynamic performance of HCCS encouraged us to further evaluate its final anti-tumor effect. Above all, the *in vitro* anti-tumor efficacy of HCCS was assessed using the MTT assay and live/dead cell staining analysis. Initially, 4T1 cells were exposed to varying concentrations of CS, HC, HC + CS, as well as HCCS. Fig. 2D demonstrated that HC exhibited nearly no cytotoxicity in the absence of light, while CS displayed minimal cytotoxicity. Despite HCCS showing significant toxicity at higher concentrations, the cell viability remained above 70%. This suggested that the differential cellular uptake of CS might contribute to these observations. However, upon light activation, HCCS exhibited potent cytotoxicity even at low concentrations, indicating a significantly superior PDT effect of HCCS over HC (Fig. 2E). Similar trends were observed in the live/dead cell staining analysis (Fig. 2F). In the absence of light, 4T1 cells treated with low concentrations of such agents retained bright green fluorescence, indicating a robust viability of tumor cells. Following HC-mediated PDT, only a few cells exhibited red fluorescence, reflecting cell death. In contrast, a substantial number of cells died and exhibited red fluorescence after HCCS treatment. We attributed the enhanced PDT of HCCS to the positive feedback loop involving CS-induced activation of AMPK and the inhibition of GSTs, which dramatically increased the cellular uptake of drugs and weakened cell resistance to PDT. Moreover, the much better anti-tumor efficiency of HCCS compared to HC + CS demonstrated enormous advantages of albumin-based drug co-delivery for efficient tumor treatment.

To explore the mechanism of HCCS for enhancing cellular uptake and oxidative stress, the activities of GSTs and AMPK in 4T1 cells were measured. Fig. 3A demonstrated that both CS and HCCS effectively suppressed GSTs activity, but the latter worked better. The reason might be the limited uptake of free CS by cells, which implied the superiority of albumin-based nanomedicine in drug delivery. Of note, the PDT of HC and HCCS was also detected to inhibit the activity of GSTs, which should be the help of ROS. Further, GSTs expression in cells was evaluated through protein immunoblotting analysis (Fig. 3B), and the band intensities were quantitatively analyzed using Image J software (Fig. 3C). Results indicated that HCCS significantly downregulated the expression level of GSTs, with the light-exposed group showing more notable inhibitory effect. Thus, it was concluded that HCCS was able to simultaneously inhibit the activity and expression of GSTs in tumor cells, thereby disturbing GSH to combat antioxidant defense systems and amplify intracellular oxidative stress.

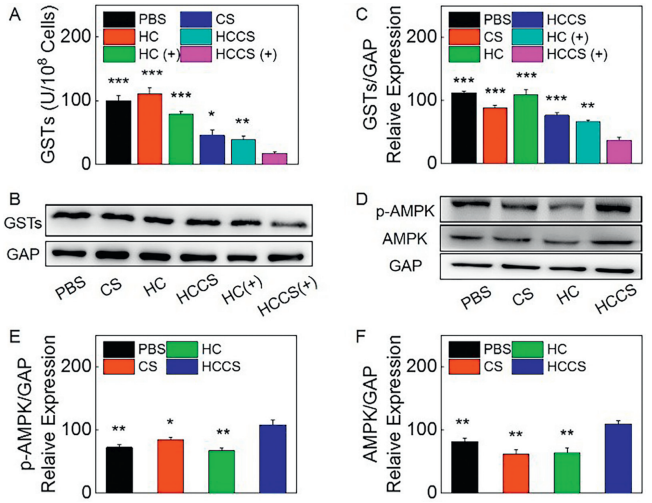

Fig. 3. Detection of GSTs and AMPK activity levels. (A) Analysis of GSTs activity in 4T1 cells treated with CS, HC and HCCS in the presence or absence of light ($n = 3$). (B) Western blot and (C) quantification analysis of GSTs expression in 4T1 cells treated with CS, HC, and HCCS in the presence or absence of light ($n = 3$). (D) Western blot analysis of AMPK and p-AMPK levels in 4T1 cells treated with CS, HC, and HCCS. Quantification of (E) p-AMPK and (F) AMPK levels in 4T1 cells treated with CS, HC, and HCCS ($n = 3$). Mean ± SD. $^{*}P < 0.05$, $^{**}P < 0.01$ and $^{***}P < 0.001$ were tested *via* a Student's *t*-test.

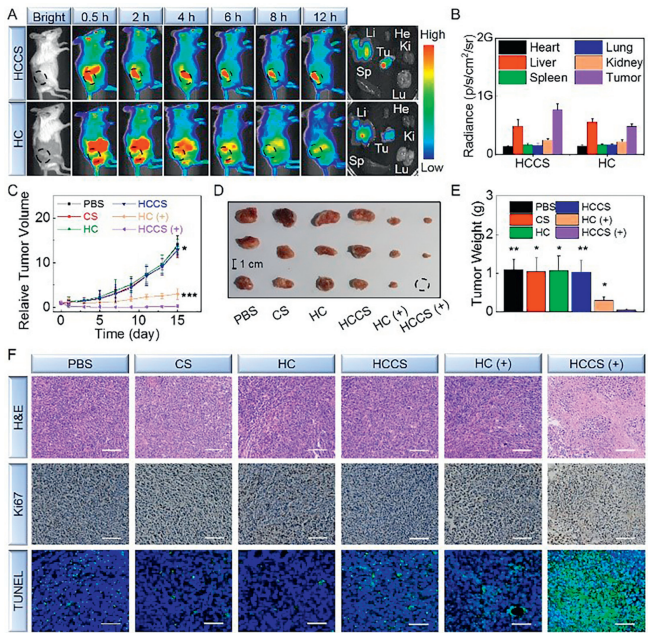

Fig. 4. *In vivo* anti-tumor study. (A) Fluorescence images of 4T1 tumor-bearing mice at 0.5, 2, 4, 6, 8, and 12 h, as well as excised organs at 12 h after intravenous injection of HC or HCCS. (B) Quantification of fluorescence in excised organs ($n = 3$). (C) Relative tumor volume changes of mice treated with CS, HC, and HCCS in the presence or absence of light for 15 days ($n = 5$). (D) Dissected tumor tissue photographs and (E) average tumor weight of different groups ($n = 3$). (F) H&E, Ki67, and TUNEL immunofluorescence staining of dissected tumor tissues. Scale bar: 100 μm. Mean ± SD. $^{*}P < 0.05$, $^{**}P < 0.01$ and $^{***}P < 0.001$ were tested *via* a Student's *t*-test.

Next, protein immunoblotting was employed to examine the activation levels of AMPK. As shown in Fig. 3D, compared with phosphate buffered saline (PBS) group, treatment with HCCS resulted in an obvious increase in phosphorylation of AMPK (p-AMPK) level, suggesting that HCCS effectively stimulated AMPK activation. Quantitative analysis of band intensities was conducted using Image J software (Figs. 3E and F). It was observed that HCCS significantly increased the expressions of p-AMPK and AMPK on 4T1 cells. AMPK played a vital role in nutrient signaling in tumor cells. HSA served as a nutrient could be actively internalized by cells *via* macropinocytosis. Consequently, HCCS triggered AMPK activation would further augment the cellular uptake of HCCS and establish a positive feedback mechanism, which greatly improved the delivery efficiency of photosensitizers for stronger PDT.

Prior to the initiation of anti-tumor treatment, the biodistribution of HCCS in mice was assessed using a small animal imager. All animal experiments were performed based on the guidelines of Institutional Animal Care and Use Committee (IACUC) of China and approved by the Animal Ethics Committee of Southern Medical University. Fig. 4A illustrated the gradual accumulation of fluorescence throughout the mouse body following the drug injection *via* the tail vein, indicating systemic distribution through the bloodstream. Subsequently, specific fluorescence accumulation was observed in the tumor tissue. Notably, even after 12 h, the preferential accumulation of fluorescence in the tumor tissue persisted, highlighting the favorable tumor targeting property of HCCS. *Ex vivo* imaging of tumors and major organs after sacrificing the tumor-bearing mice further confirmed the strongest fluorescence signal in the tumor tissue (Fig. 4B). It was worth mentioning that HCCS-treated tumors exhibited more pronounced and sustained fluorescence accumulation compared to HC-treated tumors, emphasizing the excellent tumor targeting and retention capabilities of this albumin-based nanomedicine. Effective tumor accumulation and drug retention are crucial for achieving successful tumor eradication. Although some HCCS was inevitably found in normal tissues, its low dark toxicity suggested the likelihood of minimal side effects.

Subsequently, the therapeutic effect of HCCS was investigated on solid tumor *in vivo*. Following the injection of drugs through tail vein, tumor volume was monitored at regular intervals to construct the tumor growth curve (Fig. 4C). Compared to the control group treated with PBS, HC without light exhibited almost no inhibition of tumor growth. HCCS without light and free CS demonstrated very limited tumor inhibition effects. However, upon light activation of PDT, HC-treated tumors initially exhibited inhibition but regrew after 8 days. In contrast, only HCCS maintained effective and prolonged tumor inhibition for 15 days after PDT. This could be attributed to the improved drug delivery efficiency of HCCS by effective tumor accumulation and cellular uptake, along with its ability to block the cellular antioxidant defense system by inhibiting GSTs activity, thereby enhancing the anti-tumor effect of PDT. Upon completion of the treatment, tumor tissues were excised, photographed, and weighed. Fig. 4D demonstrated that light-activated HC attenuated tumor growth, whereas HCCS exhibited more potent and persistent tumor inhibition. Additionally, the mean tumor weight was also the lowest in the group of HCCS with light (Fig. 4E). Histological examination of tumor tissues stained with hematoxylin and eosin (H&E) revealed that the tumor section treated with HCCS and light exhibited the lowest cell density, with a significant number of tumor cells lacking complete nuclei (Fig. 4F), proving effective destruction of tumor tissues by the PDT of HCCS. Furthermore, immunofluorescence staining of tumor tissue revealed weaker Ki67 fluorescence (indicating reduced tumor cell proliferation) and stronger terminal deoxynucleotidyl transferase dUTP nick end labeling (TUNEL) fluorescence (indicating increased tumor cell apoptosis) in the HCCS PDT-treated tumors. To sum up, CS-mediated AMPK activation and GSTs inhibition remarkably enhanced the PDT efficacy of HSA-based photodynamic nanoplatform through promoting the targeted drug delivery and destroying endogenous antioxidant defense systems of breast cancer.

To assess the *in vivo* biological safety of HCCS, the body weight of mice was monitored every two days throughout the treatment period. As depicted in Fig. S3 (Supporting information), the mice

exhibited stable body weight without a significant decline, indicating the low systemic toxicity of the treatment drugs. Following the completion of the treatment, blood samples were collected from the mice for biochemical analysis. The analysis of relevant biochemical indicators, such as alanine aminotransferase (ALT), aspartate aminotransferase (AST), blood urea nitrogen (BUN), and uric acid (UA), revealed that they remained within the normal ranges across different treatment groups (Fig. S4 in Supporting information). These results suggested that there was no significant impairment of liver and kidney function, despite the inevitable accumulation of the drug. Furthermore, the main organs were subjected to H&E staining (Fig. S5 in Supporting information), which demonstrated normal tissue morphology in the heart, liver, spleen, lung, and kidney. This further confirmed the minimal systemic toxicity of the therapeutic agents towards normal tissues. Blood routine analysis indicated that the major hematological parameters of the mice remained within the normal ranges following PDT, indicating good blood compatibility (Fig. S6 in Supporting information). Overall, the nanomedicine HCCS exhibited excellent biocompatibility and low side effects during the treatment process.

In conclusion, we developed an albumin nanomedicine called HCCS that facilitated positive feedback cellular uptake and inhibited GSTs activity, significantly enhancing PDT effect of breast cancer. HCCS, prepared through hydrophobic interaction, demonstrated excellent stability and dispersibility in aqueous environments. Upon tail vein injection, the nanosized HCCS selectively accumulated in tumor tissues. Following initial internalization by tumor cells, HCCS induced a positive feedback mechanism, activating AMPK to enhance cellular uptake behavior. Compared to HC + CS, HCCS also exhibited superior cellular uptake behavior and more potent PDT efficiency, highlighting the advantages of albumin-based drug co-delivery system. Importantly, HCCS was found to interfere with the antioxidant defense system of tumor cells by inhibiting GSTs activity, which amplified the intracellular oxidative stress and further enhanced the lethality of PDT to tumors. Ultimately, HCCS effectively suppressed tumor growth by integration of increasing photosensitizer delivery efficiency and combating antioxidant defense system, which shed light on developing drug-co-delivery nanoplatform for oxidative therapies of tumors.

Declaration of competing interest

The authors declare that they have no known competing financial interests or personal relationships that could have appeared to influence the work reported in this paper.

Acknowledgments

We are grateful for the financial support of National Natural Science Foundation of China (No. 52073140), and the Guangdong Basic and Applied Basic Research Foundation (No. 2022B1515020095).

Supplementary materials

Supplementary material associated with this article can be found, in the online version, at doi:10.1016/j.cclet.2023.109254.

References

[1] B.C. Zhang, L. Lin, J.Z. Mao, et al., Chin. Chem. Lett. 34 (2023) 108518.
[2] J. Xu, Y. Lai, F.Y. Wang, et al., Chin. Chem. Lett. 34 (2023) 108332.
[3] X.W. Da, X.L. Liu, C. Li, et al., Chin. Chem. Lett. 34 (2023) 108317.
[4] J.Q. Huang, L.P. Zhao, X. Zhou, et al., Small 18 (2022) 2107467.
[5] L.P. Zhao, R.R. Zheng, H.Q. Chen, et al., Nano Lett. 20 (2020) 2062–2071.
[6] X. Zhou, J.Q. Huang, L.S. Liu, et al., ACS Appl. Bio Mater. 4 (2021) 8023–8032.
[7] Y. Zhou, X. Ren, Z. Hou, et al., Nanoscale Horiz. 6 (2021) 120–131.
[8] X. Li, R. Kong, Y. Li, et al., Chem. Commun. 58 (2022) 3917–3920.
[9] Z. Chen, L. Liu, R. Liang, et al., ACS Nano 12 (2018) 8633–8645.
[10] Q. Chen, X. Wang, C. Wang, et al., ACS Nano 9 (2015) 5223–5233.
[11] Q. Chen, J. Chen, C. Liang, et al., J. Control. Release 263 (2017) 79–89.
[12] Y. Huang, N. He, Y. Wang, et al., J. Mater. Chem. B 7 (2019) 1149–1159.
[13] A. Yuan, J. Wu, C. Song, et al., J. Pharm. Sci. 102 (2013) 1626–1635.
[14] S. Lamichhane, S. Lee, Arch. Pharm. Res. 43 (2020) 118–133.
[15] H.X. Lu, L. Noorani, Y.Y. Jiang, et al., J. Mater. Chem. B 5 (2017) 9591–9599.
[16] C.R. Park, J.H. Jo, M.G. Song, et al., Theranostics 9 (2019) 7447–7457.
[17] S. Herzig, R.j. Shaw, Nat. Rev. Mol. Cell Biol. 19 (2018) 121–135.
[18] J. Yuan, X. Dong, J. Yap, et al., J. Hematol. Oncol. 13 (2020) 113.
[19] R. Li, T.S.C. Ng, S.J. Wang, et al., Nat. Nanotechnol. 16 (2021) 830–839.
[20] J.L. Figarola, S. Rahbar, Int. J. Mol. Med. 31 (2013) 1166–1176.
[21] Y.Q. Zhu, Y.H. Song, Z.Y. Cao, et al., Adv. Funct. Mater. 31 (2021) 2103655.
[22] Z.Y. Cao, D.D. Li, L. Zhao, et al., Nat. Commun. 13 (2022) 2038.
[23] S.S. Singhal, J. Figarola, J. Singhal, et al., Biochem. Pharmacol. 84 (2012) 1419–1427.
[24] A. Chatterjee, S. Gupta, Cancer Lett. 433 (2018) 33–42.
[25] E. Laborde, Cell Death Differ. 17 (2010) 1373–1380.
[26] R.R. Singh, J. Mohammad, O. Megan, et al., Cancers 12 (2020) 1501.
[27] I.R. Jowsey, A.M. Thomson, J.U. Flanagan, et al., Biochem. J. 359 (2001) 507–516.